



Supplement of

Cloud droplet formation at the base of tropical convective clouds: closure between modeling and measurement results of ACRIDICON-CHUVA

Ramon Campos Braga et al.

Correspondence to: Mira L. Pöhlker (poehlker@tropos.de) and Barbara Ervens (barbara.ervens@uca.fr)

The copyright of individual parts of the supplement might differ from the article licence.

Table S1. Geometric mean and standard deviation of atmospheric parameters measured below cloud base. Note that the mean diameter is a fit parameter of the average aerosol size distribution and the error is 15 % according to (Cai et al., 2008; Moore et al., 2021) Measurements were performed during Flight AC07, time frame of averaged below cloud period: 6-09-2014 17:53:00 to 17:55:25 UTC

Parameter	Mean \pm SD
Altitude [m asl.]	1800 \pm 0.05
Air Temperature [$^{\circ}$ C]	18 \pm 0.15
Pressure [hPa]	820 \pm 0.25
Relative Humidity [%]	95 \pm 3
N_{CN} [cm^{-3}]	2417 \pm 42
N_{UHSAS} [cm^{-3}]	2024 \pm 162
d_{acc} [nm]	147 \pm 22

Table S2. Geometric mean and standard deviation of atmospheric parameters measured below cloud base. Note that the mean diameter is a fit parameter of the average aerosol size distribution and the error is 15 % according to (Cai et al., 2008; Moore et al., 2021). Measurements were performed during Flight AC09, time frame of averaged below cloud period: 11-09-2014 15:31:31 to 15:38:20 UTC.

Parameter	Mean \pm SD
Altitude [m asl.]	933 \pm 0.05
Air Temperature [$^{\circ}$ C]	22.5 \pm 0.15
Pressure [hPa]	938 \pm 0.25
Relative Humidity [%]	87 \pm 3
N_{CN} [cm^{-3}]	737 \pm 58
N_{UHSAS} [cm^{-3}]	686 \pm 59
d_{acc} [nm]	140 \pm 22

Table S3. Geometric mean and standard deviation of atmospheric parameters measured below cloud base. Note that the mean diameter is a fit parameter of the average aerosol size distribution and the error is 15 % according to (Cai et al., 2008; Moore et al., 2021). Measurements were performed during Flight AC18, time frame of averaged below cloud period: 28-09-2014 16:39:00 to 16:43:59 UTC.

Parameter	Mean \pm SD
Altitude [m asl.]	1286 \pm 0.05
Air Temperature [$^{\circ}$ C]	20.7 \pm 0.15
Pressure [hPa]	876 \pm 0.25
Relative Humidity [%]	81.8 \pm 2
N_{CN} [cm^{-3}]	809 \pm 20
N_{UHSAS} [cm^{-3}]	707 \pm 83
d_{acc} [nm]	140 \pm 21

Table S4. Geometric mean and standard deviation of atmospheric parameters measured below cloud base. Note that the mean diameter is a fit parameter of the average aerosol size distribution and the error is 15 % according to (Cai et al., 2008; Moore et al., 2021). Measurements were performed during Flight AC19, time frame of averaged below cloud period: 30-09-2014 17:23:38 to 17:27:31 UTC.

Parameter	Mean \pm SD
Altitude [m asl.]	452 \pm 0.05
Air Temperature [$^{\circ}$ C]	23.5 \pm 0.15
Pressure [hPa]	960 \pm 0.25
Relative Humidity [%]	93.7 \pm 3
N_{CN} [cm^{-3}]	428 \pm 138
N_{UHSAS} [cm^{-3}]	227 \pm 52
N_{ait} [cm^{-3}]	\sim 201
N_{acc} [cm^{-3}]	227 \pm 52
d_{ait} [nm]	\sim 37
d_{acc} [nm]	136 \pm 20

Table S5. Cloud probe size intervals and central bin diameters during HALO flights.

Cloud Probe	Size interval	Number of bins	Central bin diameter (μm)
CCP-CDP	3-50 μm	14	3.8, 6.1, 8.7, 10.9, 13.5, 17.1, 19.7, 22.5, 25.9, 28.3, 31.7, 36.6, 40.7, 44.2
CAS-DPOL	3-50 μm	10	3.9, 6, 10.8, 17.3, 22.3, 27.4, 32.4, 37.4, 42.4, 47.4

Table S6. Cloud base thermodynamic parameters and classification of each flight.

Flight	Classification	Altitude [m asl.]	Air Temperature [$^{\circ}$ C]	Time frame of measurements [UTC]
AC07	Arc of Deforestation	1920	15	18:02:13 to 18:14:13
AC09	Remote Amazon	1200	19.5	15:40:41 to 15:58:35
AC18	Remote Amazon	1700	17	16:45:29 to 16:55:46
AC19	Atlantic Ocean	605	22	17:28:04 to 17:37:39

Table S7. Statistical parameters (bias, root mean square error - RMSE, mean absolute error - MAE, mean ratio between $N_{d,p}$ and $N_{d,m}$ - RATIO) from closure analysis of simulated droplet concentration for CCP-CDP as a function of κ for Flight AC07.

κ	BIAS (cm ⁻³)	RMSE (cm ⁻³)	MAE (cm ⁻³)	RATIO
0.05	-94.7	226.7	170.0	0.90
0.1	103.2	217.2	198.1	1.11
0.2	269.7	333.8	302.0	1.30
0.3	341.3	395.5	358.2	1.38
0.6	420.2	468.4	426.4	1.46

Table S8. Statistical parameters (bias, root mean square error - RMSE, mean absolute error - MAE, mean ratio between $N_{d,p}$ and $N_{d,m}$ - RATIO) from closure analysis of simulated droplet concentration for CAS-DPOL as a function of κ for Flight AC07.

κ	BIAS (cm ⁻³)	RMSE (cm ⁻³)	MAE (cm ⁻³)	RATIO
0.05	-315.3	357.3	315.3	0.72
0.1	-126.1	194.1	155.9	0.89
0.2	29.4	155.2	131.0	1.03
0.3	96.6	184.2	163.3	1.09
0.6	172.9	241.7	211.9	1.16

Table S9. Statistical parameters (bias, root mean square error - RMSE, mean absolute error - MAE, mean ratio between $N_{d,p}$ and $N_{d,m}$ - RATIO) from closure analysis of simulated droplet concentration for CAS-DPOL and CCP-CDP as a function of κ for Flight AC07.

κ	BIAS (cm ⁻³)	RMSE (cm ⁻³)	MAE (cm ⁻³)	RATIO
0.05	-198.2	295.3	238.2	0.80
0.1	-4.4	206.7	178.3	1.00
0.2	157.0	265.5	221.8	1.16
0.3	226.5	314.6	266.8	1.23
0.6	304.2	379.3	325.7	1.30

Table S10. Statistical parameters (bias, root mean square error - RMSE, mean absolute error - MAE, mean ratio between $N_{d,p}$ and $N_{d,m}$ - RATIO) from closure analysis of simulated droplet concentration for CCP-CDP as a function of κ for Flight AC09.

κ	BIAS (cm ⁻³)	RMSE (cm ⁻³)	MAE (cm ⁻³)	RATIO
0.05	-38.5	46.6	39.7	0.89
0.1	54.9	60.4	56.4	1.16
0.2	141.4	145.1	141.4	1.41
0.3	188.5	192.7	188.5	1.55
0.6	247.4	252.6	247.4	1.72

Table S11. Statistical parameters (bias, root mean square error - RMSE, mean absolute error - MAE, mean ratio between $N_{d,p}$ and $N_{d,m}$ - RATIO) from closure analysis of simulated droplet concentration for CAS-DPOL as a function of κ for Flight AC09.

κ	BIAS (cm ⁻³)	RMSE (cm ⁻³)	MAE (cm ⁻³)	RATIO
0.05	-165.3	171.5	165.3	0.65
0.1	-72.1	81.0	74.9	0.85
0.2	13.9	35.2	24.8	1.03
0.3	61.0	72.7	63.0	1.13
0.6	119.1	129.0	119.1	1.25

Table S12. Statistical parameters (bias, root mean square error - RMSE, mean absolute error - MAE, mean ratio between $N_{d,p}$ and $N_{d,m}$ - RATIO) from closure analysis of simulated droplet concentration for CAS-DPOL and CCP-CDP as a function of κ for Flight AC09.

κ	BIAS (cm ⁻³)	RMSE (cm ⁻³)	MAE (cm ⁻³)	RATIO
0.05	-95.1	119.7	95.8	0.76
0.1	-1.8	70.3	64.6	1.00
0.2	84.5	110.5	89.4	1.21
0.3	131.6	151.4	132.5	1.33
0.6	190.1	206.8	190.1	1.47

Table S13. Statistical parameters (bias, root mean square error - RMSE, mean absolute error - MAE, mean ratio between $N_{d,p}$ and $N_{d,m}$ - RATIO) from closure analysis of simulated droplet concentration for CCP-CDP as a function of κ for Flight AC18.

κ	BIAS (cm ⁻³)	RMSE (cm ⁻³)	MAE (cm ⁻³)	RATIO
0.05	-94.7	226.7	170.0	0.90
0.1	103.2	217.2	198.1	1.11
0.2	269.7	333.8	302.0	1.30
0.3	341.3	395.5	358.2	1.38
0.6	420.2	468.4	426.4	1.46

Table S14. Statistical parameters (bias, root mean square error - RMSE, mean absolute error - MAE, mean ratio between $N_{d,p}$ and $N_{d,m}$ - RATIO) from closure analysis of simulated droplet concentration for CAS-DPOL as a function of κ for Flight AC18.

κ	BIAS (cm ⁻³)	RMSE (cm ⁻³)	MAE (cm ⁻³)	RATIO
0.05	-156.8	167.6	156.8	0.68
0.1	-88.8	106.0	89.5	0.82
0.2	-25.1	67.1	57.8	0.95
0.3	5.4	66.8	58.6	1.01
0.6	47.9	90.2	73.6	1.10

Table S15. Statistical parameters (bias, root mean square error - RMSE, mean absolute error - MAE, mean ratio between $N_{d,p}$ and $N_{d,m}$ - RATIO) from closure analysis of simulated droplet concentration for CAS-DPOL and CCP-CDP as a function of κ for Flight AC18.

κ	BIAS (cm ⁻³)	RMSE (cm ⁻³)	MAE (cm ⁻³)	RATIO
0.05	-90.2	125.3	101.5	0.79
0.1	-21.7	89.9	75.9	0.95
0.2	42.6	101.1	83.5	1.10
0.3	73.4	120.0	99.6	1.17
0.6	116.2	154.7	128.8	1.28

Table S16. Statistical parameters (bias, root mean square error - RMSE, mean absolute error - MAE, mean ratio between $N_{d,p}$ and $N_{d,m}$ - RATIO) from closure analysis of simulated droplet concentration for CCP-CDP as a function of κ_{Ait} and κ_{acc} for Flight AC19.

κ_{Ait}	κ_{acc}	BIAS (cm^{-3})	RMSE (cm^{-3})	MAE (cm^{-3})	RATIO
0.05	0.05	-27.0	30.3	27.0	0.83
0.1	0.1	8.1	18.9	16.4	1.05
0.2	0.2	39.1	45.7	41.0	1.24
0.3	0.3	54.3	60.5	55.0	1.34
0.6	0.6	74.6	80.0	74.6	1.46
0.1	0.6	19.1	22.7	20.1	1.12
0.1	0.8	26.7	30.0	27.7	1.17
0.2	0.6	46.0	48.8	46.0	1.29
0.2	0.8	52.6	54.6	52.6	1.33

Table S17. Statistical parameters (bias, root mean square error - RMSE, mean absolute error - MAE, mean ratio between $N_{d,p}$ and $N_{d,m}$ - RATIO) from closure analysis of simulated droplet concentration for CAS-DPOL as a function of κ_{Ait} and κ_{acc} for Flight AC19.

κ_{Ait}	κ_{acc}	BIAS (cm^{-3})	RMSE (cm^{-3})	MAE (cm^{-3})	RATIO
0.05	0.05	-100.6	103.9	100.6	0.53
0.1	0.1	-65.6	70.3	65.6	0.69
0.2	0.2	-31.8	44.2	34.5	0.85
0.3	0.3	-14.4	38.1	26.9	0.93
0.6	0.6	9.1	40.9	34.4	1.04
0.1	0.6	-58.3	60.7	58.3	0.73
0.1	0.8	-53.0	54.9	53.0	0.75
0.2	0.6	-27.4	35.8	30.0	0.87
0.2	0.8	-23.0	29.7	25.5	0.89

Table S18. Statistical parameters (bias, root mean square error - RMSE, mean absolute error - MAE, mean ratio between $N_{d,p}$ and $N_{d,m}$ - RATIO) from closure analysis of simulated droplet concentration for CAS-DPOL and CCP-CDP as a function of κ_{Ait} and κ_{acc} for Flight AC19.

κ_{Ait}	κ_{acc}	BIAS (cm^{-3})	RMSE (cm^{-3})	MAE (cm^{-3})	RATIO
0.05	0.05	-61.8	74.8	61.8	0.67
0.1	0.1	-26.8	50.3	39.7	0.86
0.2	0.2	5.5	45.0	37.9	1.03
0.3	0.3	21.8	51.1	41.7	1.12
0.6	0.6	43.6	64.5	55.5	1.23
0.1	0.6	-17.5	44.9	38.2	0.91
0.1	0.8	-11.1	43.6	39.7	0.94
0.2	0.6	11.3	43.1	38.4	1.06
0.2	0.8	16.9	44.6	39.8	1.09

S1 Atmospheric conditions below and at cloud base during flight AC19

In this section, we give details on the characterization of the atmospheric conditions, under which the aerosol and cloud microphysical data used in this study were obtained during flight AC19 (30 Sep 2014) within the overall scientific scope of the ACRIDICON-CHUVA campaign (Wendisch et al., 2016; Braga et al., 2017; Cecchini et al., 2017). The flight track of AC19 followed the Amazon River valley from Manaus to the Amazon River delta with cloud profiling maneuvers over the Atlantic Ocean near the Brazilian coast. During the cloud profiling, the experimental data for AC19 were obtained. A map showing the whole flight track as well as backward trajectories (BTs) for the cloud profiling period (about 17:23 to 17:37 UTC) within the region of interest (ROI_{profil}) is shown in Figure S1.

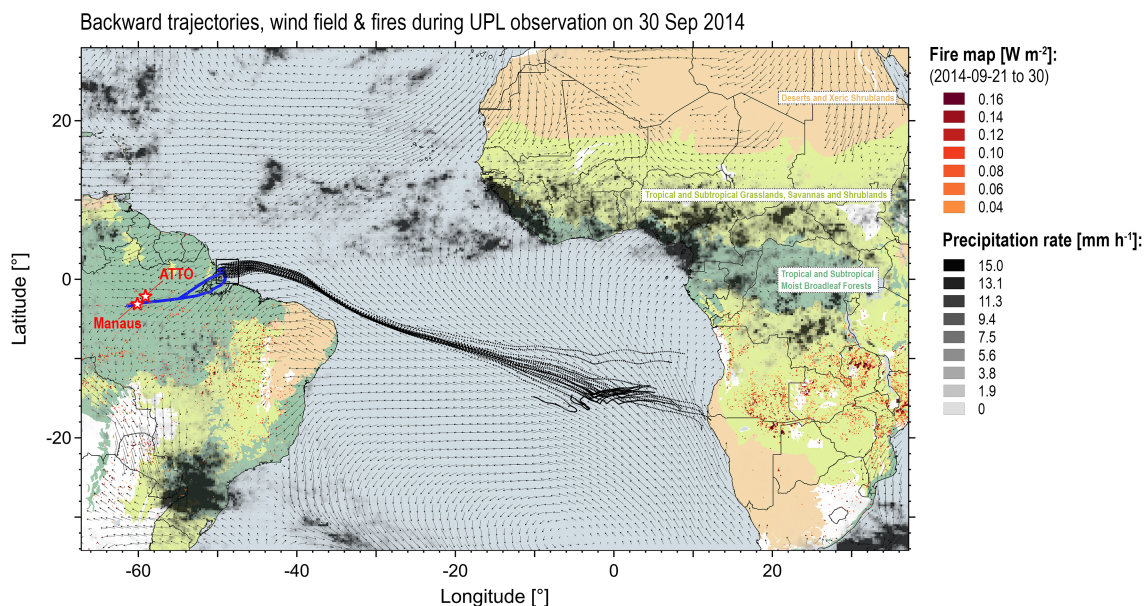


Figure S1. Map combining the entire flight track (blue) and backward trajectories (HYSPLIT, GDAS0.5, 9 days, start height 200 m above sea level, shown in black) during of flight AC19 on 30 September 2014. HYSPLIT backward trajectories started at 18:00 UTC, corresponding to the period of the offshore cloud profiling maneuvers. The geographic locations of the city of Manaus as well as the ATTO site Andreae et al. (2015) are shown as red markers. For the 9-day backward trajectory time window (21 to 30 of Sep 2014) averaged data on: (i) fire radiative power density ($mW m^{-2}$) retrieved by the Global Fire Assimilation System (GFAS v1.0) as well as (ii) TRMM precipitation rates are shown.

The backward trajectories (BTs) in Figure S1 indicate an advection of the air masses, which were observed in the marine boundary layer (MBL) within the ROI_{profil} , from southeastern directions and further suggest that the air spent about 9 days over the ocean without being influenced by emissions from the South American continent. The BTs point towards Africa, which is a major source of biomass burning (BB) pollution during this time of the year (i.e., August and September) (Holanda et al., 2020; Katich et al., 2018). Accordingly, Figure S1 suggests that the air masses probed in the ROI_{profil} were primarily influenced by African biomass burning. These air masses underwent long-range transport across the Atlantic Ocean during which they experienced ocean-atmosphere exchange. This means that the air masses and aerosol populations probed below and at cloud base in the ROI_{profil} presumably represent MBL conditions, with a certain amount of aged African BB pollution.

The related study by Holanda et al. (2020) - which focused on the same flight AC19 - observed transatlantic transport of African BB pollution into the Amazon Basin. A remarkable finding of this study was a pronounced vertical stratification of the troposphere over the ocean with a well-defined upper pollution layer at about 3.5 km, a clean layer at about 3.2 km, and a comparatively broad lower pollution layer between 2 and 3 km. While these layers between 2 and 4 km were well-defined and mostly decoupled from the MBL over the ocean, they started to broaden and to subside upon moving above the continent, due

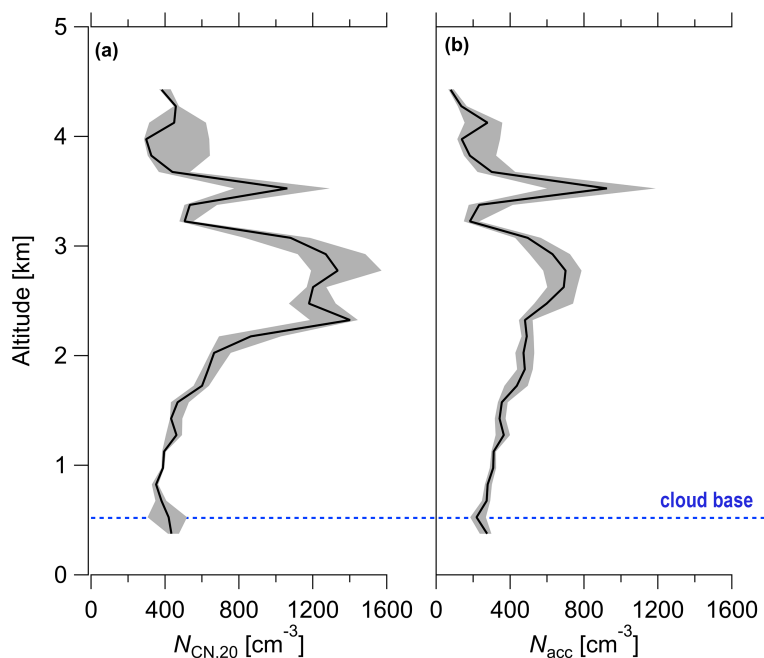


Figure S2. Tropospheric profiles of the selected aerosol properties: total particle concentration, $N_{CN,20}$, particle concentration in the accumulation mode, N_{acc} , and CCN concentration at a water vapor supersaturation of 0.5%, $N_{CCN}(0.5\%)$, during AC19, adapted from Holanda et al. (2020). Profiles show pronounced tropospheric stratification with enriched pollution between about 2 and 4 km as well as a comparatively clean marine boundary layer below cloud base at about 500 m. Further profiles from offshore measurements during AC19 on meteorological, aerosol, and trace gas parameters can be found in (Holanda et al., 2020)

to convective mixing and entrainment. Along these lines, the tropospheric profiles in Figure S2 suggest that the MBL below cloud base (i.e., below 500 m) was comparatively clean given the strongly enriched pollution in the layers above.

During the cloud profiling, marine shallow cumulus clouds were analyzed. A satellite image of the cloud scenery on 30 September 2014 at 16:45 UTC - which was about one hour prior to the AC19 cloud profiling period (30 Sep 2014 17:25 to 19:00 UTC) - is shown in Figure S3. In combination with the flight track of AC19, Figure S3 clearly shows the particular cloud street that was probed and, thus, represents the experimental basis of this work.

For this flight the integral of a mono-modal lognormal fit of the mean aerosol size distribution (ASD) measured with a Ultra-High Sensitivity Aerosol Spectrometer (UHSAS; Droplet Measurement Technologies, Inc., Longmont, CO, USA) was much lower than the total particle number concentration in the size range of ~ 10 nm to ~ 500 nm (N_{CN}). This is a strong indication of an Aitken mode. Figure S4 shows aerosol size distributions for oceanic aerosol from literature (Wex et al., 2016; Quinn et al., 2017; Gong et al., 2019), most of these ASDs show a dominant Aitken mode. Consequently, the average shape of Aitken modes from literature was used as the shape of Aitken mode during AC19. The differences between accumulation mode particle concentration and total aerosol particle concentration measured during AC19 was used as the number concentration of Aitken mode particles during AC19.

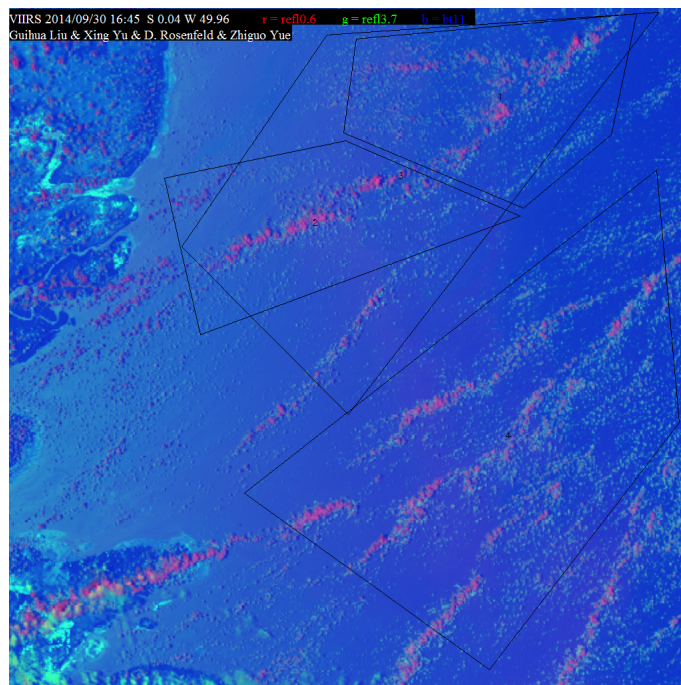


Figure S3. Satellite image from Visible Infrared Imaging Radiometer Suite (VIIRS) onboard the Suomi National Polar-Orbiting Partnership (Suomi NPP) spacecraft. VIIRS image was taken on 30 September 2014 at 16:45 UTC, which was within about one hour to the AC19 cloud profiling period. The combination with flight track demonstrates the particular cloud street that was probed during AC19.

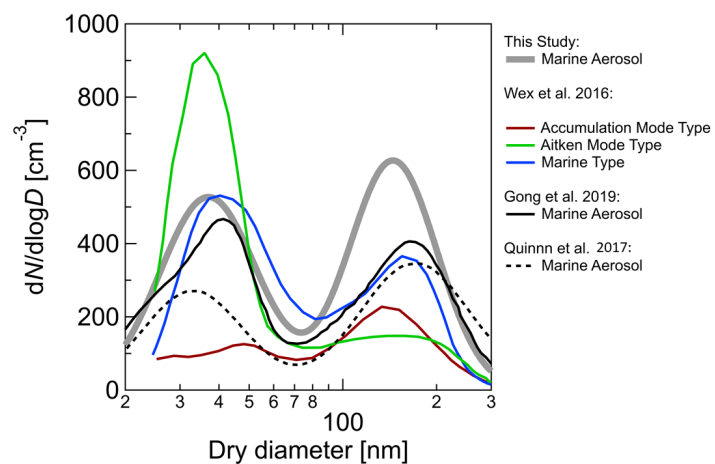


Figure S4. Aerosol size distributions from literature which was used to construct the Aitken mode size distribution for the marine air masses measured during AC19 and the final aerosol size distribution which have been used for the model of marine air masses Wex et al. (2016); Quinn et al. (2017); Gong et al. (2019).

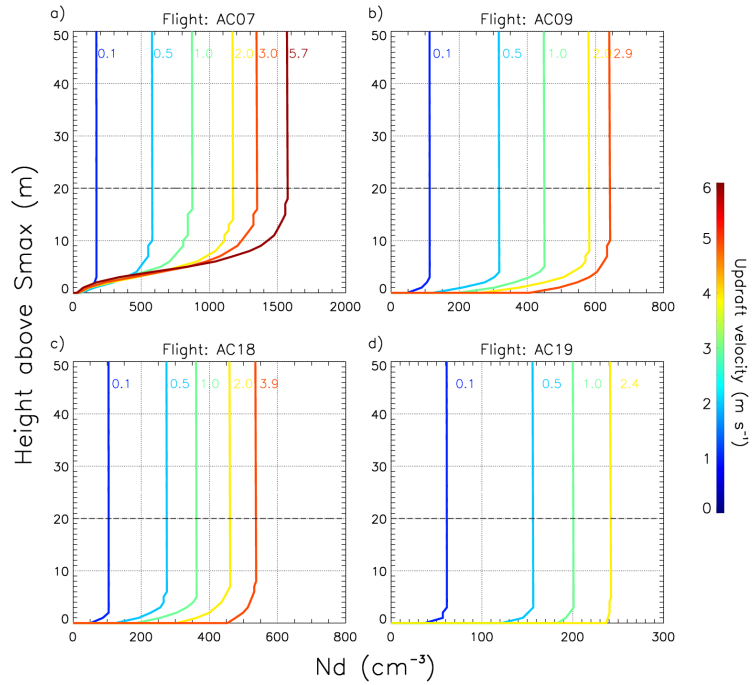


Figure S5. Predicted N_d for heights above the level of S_{max} as a function of w [m s⁻¹] (indicated on the right side of each line) for flights: a) AC07, b) AC09, c) AC18 and d) AC19. The w values correspond to ranges of measured values during cloud passes near cloud bases during each flight. The horizontal dashed line indicates the level of 20 m above S_{max} at which the cloud droplet number closure was performed.

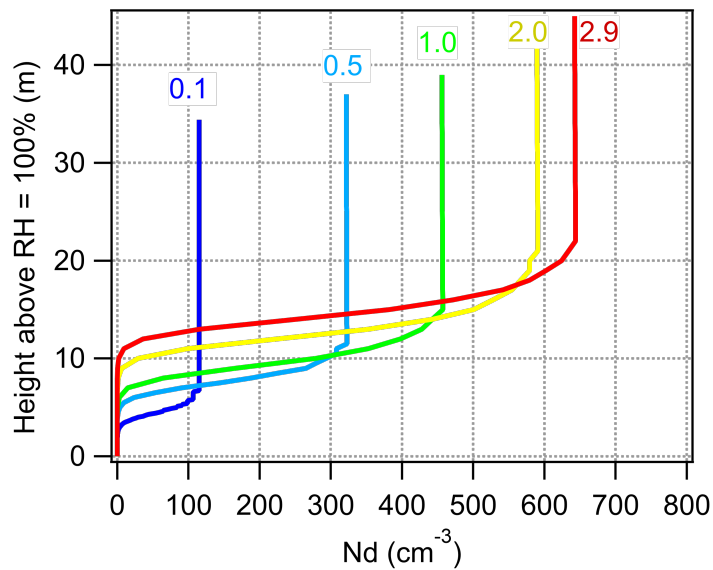


Figure S6. Predicted N_d for AC09 at heights [m] above the level at which RH = 100% in order to demonstrate the various absolute heights above S_{max} as a function of updraft speed. These are the same $N_{d,p}$ values as shown in Figure S6b. Updraft speeds in m s⁻¹ are indicated at the top of the colored lines.

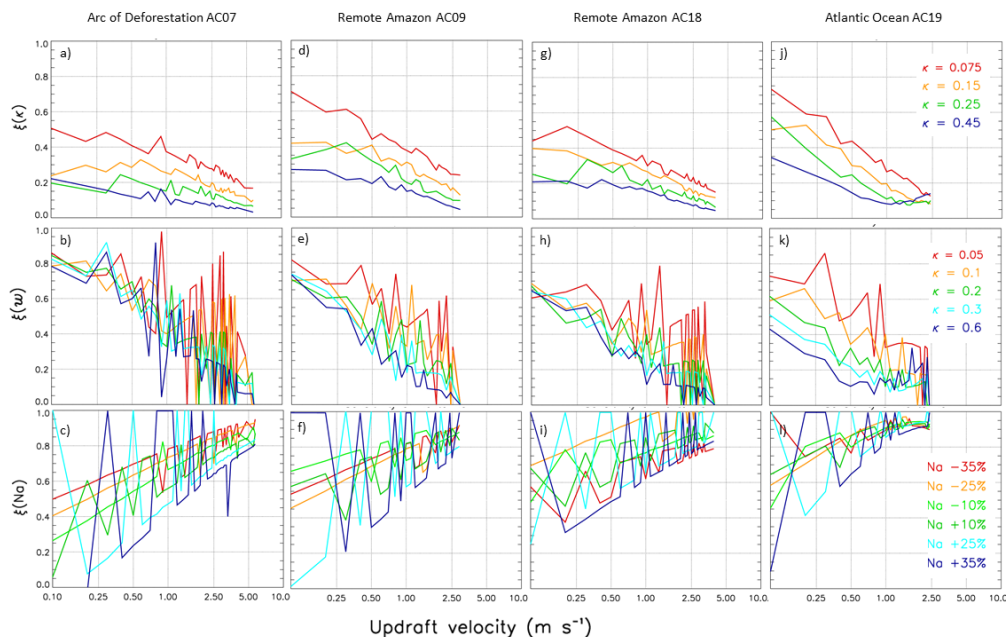


Figure S7. Modeled sensitivity of droplet number concentration (N_d) to changes in the hygroscopicity parameter κ , vertical velocity (w) and aerosol number concentration (N_a) for the measured conditions during flight AC07 (arc of deforestation), AC09 and AC18 (remote Amazon) and AC19 (Atlantic ocean).

References

- Andreae, M. O., Acevedo, O. C., Araùjo, A., Artaxo, P., Barbosa, C. G. G., Barbosa, H. M. J., Brito, J., Carbone, S., Chi, X., Cintra, B. B. L., da Silva, N. F., Dias, N. L., Dias-Júnior, C. Q., Ditas, F., Ditz, R., Godoi, A. F. L., Godoi, R. H. M., Heimann, M., Hoffmann, T., Kesselmeier, J., Könemann, T., Krüger, M. L., Lavric, J. V., Manzi, A. O., Moran-Zuloaga, D., Nölscher, A. C., Santos Nogueira, D., Piedade, M. T. F., Pöhlker, C., Pöschl, U., Rizzo, L. V., Ro, C. U., Ruckteschler, N., Sá, L. D. A., Sá, M. D. O., Sales, C. B., Santos, R. M. N. D., Saturno, J., Schöngart, J., Sörgel, M., de Souza, C. M., de Souza, R. A. F., Su, H., Targhetta, N., Tóta, J., Trebs, I., Trumbore, S., van Eijck, A., Walter, D., Wang, Z., Weber, B., Williams, J., Winderlich, J., Wittmann, F., Wolff, S., and Yáñez-Serrano, A. M.: The Amazon Tall Tower Observatory (ATTO): overview of pilot measurements on ecosystem ecology, meteorology, trace gases, and aerosols, *Atmos. Chem. Phys.*, 15, 10 723–10 776, <https://doi.org/10.5194/acp-15-10723-2015>, 2015.
- Braga, R. C., Rosenfeld, D., Weigel, R., Jurkat, T., Andreae, M. O., Wendisch, M., Pöschl, U., Voigt, C., Mahnke, C., Borrmann, S., Albrecht, R. I., Molleker, S., Vila, D. A., Machado, L. A. T., and Grulich, L.: Further evidence for CCN aerosol concentrations determining the height of warm rain and ice initiation in convective clouds over the Amazon basin, *Atmos. Chem. Phys.*, 17, 14 433–14 456, <https://doi.org/10.5194/acp-17-14433-2017>, 2017.
- Cai, Y., Montague, D. C., Mooiweer-Bryan, W., and Deshler, T.: Performance characteristics of the ultra high sensitivity aerosol spectrometer for particles between 55 and 800 nm: Laboratory and field studies, *Journal of Aerosol Science*, 39, 759–769, <https://doi.org/10.1016/j.jaerosci.2008.04.007>, 2008.
- Cecchini, M. A., Machado, L. A., Andreae, M. O., Martin, S. T., Albrecht, R. I., Artaxo, P., Barbosa, H. M., Borrmann, S., Fütterer, D., Jurkat, T., Mahnke, C., Minikin, A., Molleker, S., Pöhlker, M. L., Pöschl, U., Rosenfeld, D., Voigt, C., Weinzierl, B., and Wendisch, M.: Sensitivities of Amazonian clouds to aerosols and updraft speed, *Atmospheric Chemistry and Physics*, 17, 10 037–10 050, <https://doi.org/10.5194/acp-17-10037-2017>, 2017.
- Gong, X., Wex, H., Müller, T., Wiedensohler, A., Höhler, K., Kandler, K., Ma, N., Dietel, B., Schiebel, T., Möhler, O., and Stratmann, F.: Characterization of aerosol properties at Cyprus, focusing on cloud condensation nuclei and ice-nucleating particles, *Atmospheric Chemistry and Physics*, 19, 10 883–10 900, <https://doi.org/10.5194/acp-19-10883-2019>, 2019.

- Holanda, B. A., Pöhlker, M. L., Walter, D., Saturno, J., Sörgel, M., Ditas, J., Ditas, F., Schulz, C., Aurélio Franco, M., Wang, Q., Donth, T., Artaxo, P., Barbosa, H. M., Borrmann, S., Braga, R., Brito, J., Cheng, Y., Dollner, M., Kaiser, J. W., Klimach, T., Knote, C., Krüger, O. O., Fütterer, D., t.V. Lavric, J., Ma, N., MacHado, L. A., Ming, J., Morais, F. G., Paulsen, H., Sauer, D., Schlager, H., Schneider, J., Su, H., Weinzierl, B., Walser, A., Wendisch, M., Ziereis, H., Zöger, M., Pöschl, U., Andreae, M. O., and Pöhlker, C.: Influx of African biomass burning aerosol during the Amazonian dry season through layered transatlantic transport of black carbon-rich smoke, *Atmospheric Chemistry and Physics*, 20, 4757–4785, <https://doi.org/10.5194/acp-20-4757-2020>, 2020.
- Katich, J. M., Samset, B. H., Bui, T. P., Dollner, M., Froyd, K. D., Campuzano-Jost, P., Nault, B. A., Schroder, J. C., Weinzierl, B., and Schwarz, J. P.: Strong Contrast in Remote Black Carbon Aerosol Loadings Between the Atlantic and Pacific Basins, *Journal of Geophysical Research: Atmospheres*, 123, 13,386–13,395, <https://doi.org/10.1029/2018jd029206>, <https://agupubs.onlinelibrary.wiley.com/doi/abs/10.1029/2018JD029206>, 2018.
- Moore, R. H., Wiggins, E. B., Ahern, A. T., Zimmerman, S., Montgomery, L., Campuzano Jost, P., Robinson, C. E., Ziemba, L. D., Winstead, E. L., Anderson, B. E., Brock, C. A., Brown, M. D., Chen, G., Crosbie, E. C., Guo, H., Jimenez, J. L., Jordan, C. E., Lyu, M., Nault, B. A., Rothfuss, N. E., Sanchez, K. J., Schueneman, M., Shingler, T. J., Shook, M. A., Thornhill, K. L., Wagner, N. L., and Wang, J.: Sizing Response of the Ultra-High Sensitivity Aerosol Size Spectrometer (UHSAS) and Laser Aerosol Spectrometer (LAS) to Changes in Submicron Aerosol Composition and Refractive Index, *Atmospheric Measurement Techniques Discussions*, 2021, 1–36, <https://doi.org/10.5194/amt-2021-21>, 2021.
- Quinn, P. K., Coffman, D. J., Johnson, J. E., Upchurch, L. M., and Bates, T. S.: Small fraction of marine cloud condensation nuclei made up of sea spray aerosol, *Nature Geoscience*, 10, 674–679, <https://doi.org/10.1038/ngeo3003>, 2017.
- Wendisch, M., Pöschl, U., Andreae, M. O., Machado, L. A. T., Albrecht, R., Schlager, H., Rosenfeld, D., Martin, S. T., Abdelmonem, A., Afchine, A., Araújo, A., Artaxo, P., Aufmhoff, H., Barbosa, H. M. J., Borrmann, S., Braga, R., Buchholz, B., Cecchini, M. A., Costa, A., Curtius, J., Dollner, M., Dorf, M., Dreiling, V., Ebert, V., Ehrlich, A., Ewald, F., Fisch, G., Fix, A., Frank, F., Fütterer, D., Heckl, C., Heidelberg, F., Hüneke, T., Jäkel, E., Järvinen, E., Jurkat, T., Kanter, S., Kästner, U., Kenntner, M., Kesselmeier, J., Klimach, T., Knecht, M., Kohl, R., Kölling, T., Krämer, M., Krüger, M., Krisna, T. C., Lavric, J. V., Longo, K., Mahnke, C., Manzi, A. O., Mayer, B., Mertes, S., Minikin, A., Molleker, S., Münch, S., Nillius, B., Pfeilsticker, K., Pöhlker, C., Roiger, A., Rose, D., Rosenow, D., Sauer, D., Schnaiter, M., Schneider, J., Schulz, C., de Souza, R. A. F., Spanu, A., Stock, P., Vila, D., Voigt, C., Walser, A., Walter, D., Weigel, R., Weinzierl, B., Werner, F., Yamasoe, M. A., Ziereis, H., Zinner, T., and Zöger, M.: The ACRIDICON-CHUVA campaign: Studying tropical deep convective clouds and precipitation over Amazonia using the new German research aircraft HALO, *Bulletin of the American Meteorological Society*, p. 160128144638003, <https://doi.org/10.1175/BAMS-D-14-00255.1>, 2016.
- Wex, H., Dieckmann, K., Roberts, G. C., Conrath, T., Izaguirre, M. A., Hartmann, S., Herenz, P., Schäfer, M., Ditas, F., Schmeissner, T., Henning, S., Wehner, B., Siebert, H., and Stratmann, F.: Aerosol arriving on the Caribbean island of Barbados: Physical properties and origin, *Atmospheric Chemistry and Physics*, 16, 14 107–14 130, <https://doi.org/10.5194/acp-16-14107-2016>, 2016.